PHYSICAL REVIEW B **82**, 041308(R) (2010)

Stimulated Raman scattering in silicon photonic crystal waveguides under continuous excitation

X. Checoury,* Z. Han, and P. Boucaud
Institut d'Électronique Fondamentale, Univ. Paris Sud, CNRS UMR 8622, Bât. 220, F-91405 Orsay Cedex, France
(Received 11 April 2010; revised manuscript received 9 July 2010; published 26 July 2010)

We experimentally show that doubly resonant cavities formed by very narrow silicon photonic crystal waveguides lead to stimulated Raman scattering at room temperature under continuous excitation. The Raman gain deduced from the measurements agrees with the calculated one. The model, which accounts for stimulated scattering, two-photon absorption and free-carrier absorption, allows us to predict the onset of Raman lasing in silicon photonic crystals.

DOI: 10.1103/PhysRevB.82.041308 PACS number(s): 78.30.Am, 42.65.Dr, 42.70.Qs

Recently, there has been an increasing interest for spontaneous and stimulated Raman scattering in semiconductor photonic crystal (PhC) waveguides.[1–4] These structures are good candidates to allow the realization of ultracompact silicon Raman light amplifiers and lasers since they increase light-matter interactions. Indeed, stimulated Raman scattering can be effectively used to achieve a laser emission in silicon devices,[5–7] although the cavities used so far were quite long (more than 1 cm). To date, most of the Raman-scattering experiments in photonic crystal waveguides have been done in so-called W1 waveguides made by omitting to drill one row of holes in the ΓK direction of an otherwise perfect photonic crystal.[1,3,4] These structures, that are resonant at the Stokes frequency only, allow to observe stimulated Raman scattering under pulsed excitation.[2] However, no stimulated Raman scattering under continuous excitation has been reported so far because the Raman-scattering efficiency is not high enough in these waveguides as compared to the efficiency of other detrimental nonlinear effects such as two-photon absorption and photogenerated free-carrier absorption. One way to increase the spontaneous and stimulated Raman-scattering efficiency is to reduce the modal volume of the pump and Stokes modes while maintaining a good overlap as well as a long interaction time between the Stokes and pump modes.[8–10] As a consequence, structures resonating at both the pump and Stokes wavelengths should be studied preferentially. In this work, we show that PhC waveguides with reduced width can lead to such doubly resonant structures. In particular, we investigate spontaneous and stimulated Raman scattering in very narrow W0.66 waveguides, the width of which is equal to two-third of the W1 standard width. We show that these waveguides, that have not been studied for Raman emission so far, lead to stimulated Raman scattering under continuous pump excitation.

We investigate spontaneous and stimulated Raman scattering in very narrow W0.66 waveguides. These waveguides, whose width is equal to $0.66\sqrt{3}a$ with a the PhC period, are narrower than W1 ones whose width is equal to $\sqrt{3}a$. Figure 1 (continuous black curve) shows the calculated dispersion diagram in TE polarization of a W0.66 slab waveguide made in slab with a $0.46a$ thickness. As seen, the fundamental mode has a small group velocity near the normalized frequency of 0.26, i.e., near the low-frequency cutoff of the waveguide. For a photonic crystal of period $a=438$ nm, as in the experiment, this small group velocity occurs at the wavelength $\lambda=a/0.26=1685$ nm. However, contrary to the W1 waveguide, the W0.66 waveguides have a second low group-velocity region near the normalized frequency 0.284 that can be used to increase the interaction of the pump with the silicon. Indeed, in silicon, the Raman shift between the pump and Stokes modes is equal to 15.6 THz, which correspond to a normalized frequency shift of 0.0228 for a PhC period of 438 nm. The frequency difference between the two slow group-velocity modes is thus almost matched to the Raman shift. To further reduce the group velocity of the pump mode and better match this frequency difference to the Raman shift, we have shifted the second row of holes away from the waveguide core (Fig. 1 inset). The dashed curve shows the dispersion of the fundamental mode in the case of a $0.06\sqrt{3}a$ shift (Fig. 1). As seen, the high-frequency cutoff is lowered and the group index of the pump mode increases from 5 to 25 showing the effectiveness of the method to tune the frequency difference between the two low group-velocity modes. Moreover, at the same time, the wave vector at which the group velocity vanishes is increased and is shifted almost below the light cone.

Because of crystal symmetry in silicon, selection rules

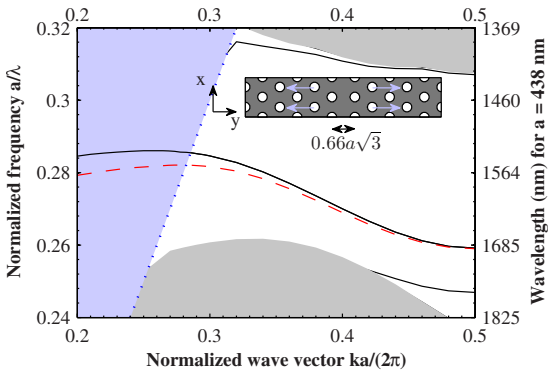

FIG. 1. (Color online) Projected band diagram of the W0.66 silicon PhC waveguide calculated by a 3D plane-wave method. The slab thickness is $0.46a$ and the hole radius $0.25a$. The light cone is represented by a dotted line. The fundamental mode of the unmodified W0.66 waveguide is represented in black. The dashed curve represents the dispersion curve of the fundamental mode when the second row of holes is shifted by $0.06\sqrt{3}a$. Inset: schematic view of the W0.66 waveguide. The arrows indicate the holes that are shifted and the direction of the shift.

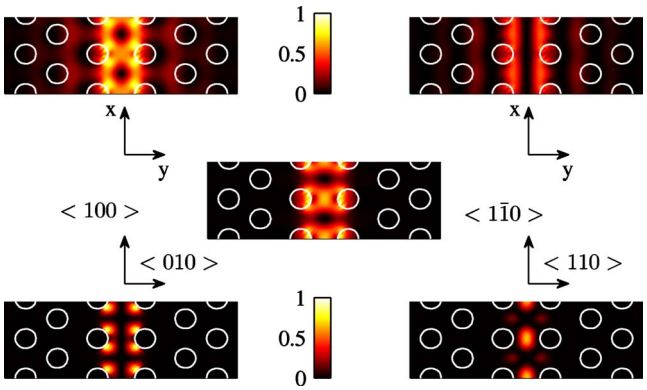

FIG. 2. (Color online) Top: pattern of the pump **E**-field squared magnitude $|\mathbf{E}_p|^2$ (left) and of the longitudinal component $|E_{px}|^2$ along the waveguide direction (x direction) (right). Middle: field pattern of the Stokes mode $|\mathbf{E}_s|^2$. Bottom: pattern of the Raman-induced polarization for a waveguide oriented in [100] (left) and [110] (right) crystallographic directions of silicon. The fields are represented at the center of the membrane (z direction) and they are calculated using a 3D plane-wave method.

impose the Raman-scattering geometries that are allowed.[11] In particular, plane waves propagating in the [110] crystallographic directions of silicon and polarized along the [1$\bar{1}$0] directions, produce a strong Raman scattering propagating with the same direction and polarization as the pump, contrary to plane waves propagating in the [100] directions and polarized along the [010] that do not. As a consequence, in the previous studies on silicon W1 PhC waveguides[3,4,10] or on narrow ridge waveguides,[7,12–14] the waveguides were oriented in the [110] direction because in these waveguides the **E** field is almost perpendicular to the waveguide axis. However, W0.66 waveguides are much narrower than W1 waveguides. The magnitudes of the longitudinal and transverse components of the **E** field have been calculated using a three-dimensional (3D) plane-wave method and are almost identical as seen in Fig. 2 (top) where the calculated pattern of the squared magnitude, $|\mathbf{E}_p|^2$, and the longitudinal component, along the x direction, $|E_{px}|^2$ of the pump **E** field are represented. As seen, the longitudinal component is responsible for almost one-third of the squared magnitude of the **E** field. This indicates that the **E** field nearly forms a 55° angle with the waveguide axis, contrary to W1 waveguides. The presence of this strong longitudinal electric field is similar to the one encountered in silicon nanowire waveguides.[15] To maximize Raman scattering, we calculated the Raman-induced polarization for the W0.66 oriented along the orientations [100] and [110] of the silicon crystal in the case where the Stokes field $\mathbf{E}_s$ corresponds to the slow mode at the low-frequency cutoff of the W0.66 (Fig. 2, middle). Figure 2 (bottom) shows the squared modulus of the Raman-induced polarization for the two crystallographic orientations. The maximum amplitude of the Raman polarization is higher in the [100] orientation as compared to the [110] orientation. To be more specific, we have calculated the associated Raman volume since the gain and the spontaneous emission rate in the PhC are inversely proportional to this volume.[8–10] The Raman volume, that represents a measure of

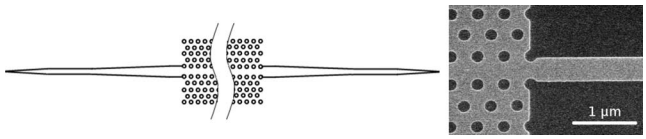

FIG. 3. Left: schematic view of the whole structure. Right: scanning electron microscope view of the PhC waveguide entrance with its access waveguide.

the Stokes and pump field overlap, is given by

$$V_R = \frac{\int \varepsilon_s(\mathbf{r})|\mathbf{E}_s(\mathbf{r})|^2 d^3r \cdot \int \varepsilon_p(\mathbf{r})|\mathbf{E}_p(\mathbf{r})|^2 d^3r}{n_p^2 n_s^2 \int_{\mathrm{Si}} \mathbf{E}_s^*(\mathbf{r})\xi_{ijkl}^{(3)}\mathbf{E}_p(\mathbf{r})\mathbf{E}_p^*(\mathbf{r})\mathbf{E}_s(\mathbf{r})d^3r},$$

where $\varepsilon_{s(p)}$ is the relative permittivity, $n_{s(p)}$ is the refractive index of silicon at Stokes (pump) wavelength, and the integral of the denominator is on the silicon volume only. Because all the nonzero components of the Raman susceptibility tensor $\chi_{ijkl}^{(3)}$ have the same magnitude in silicon, we have noted $\xi_{ijkl}^{(3)}$ the tensor the components of which equal 0, if the corresponding components of $\chi_{ijkl}^{(3)}$ are zero, and 1 otherwise. The calculated Raman volume is equal to 1×10^{-19} m^3 for one period of PhC waveguide oriented along the [100] direction and to 1.6×10^{-19} m^3 for the [110] orientation. This shows that the Raman scattering will be 1.6 times higher in the [100] orientation than in the [110] for the same design of the PhC W0.66 waveguide.

The studied cavities are made by a 50-μm-long PhC W0.66 waveguide oriented along the [100] direction of a silicon-on-insulator wafer with a 200-nm-thick Si layer on a 2-μm-thick oxide layer which was removed after the processing of the structures. The suspended W0.66 waveguides were fabricated in a triangular lattice pattern along the ΓK direction. The designed photonic crystals have a lattice period a of 438 nm and an air hole radius equal to $0.25a$ as in the simulations (Fig. 3). To improve light injection and collection through lensed fibers and to reduce optical reflections, light was injected into the W0.66 through two suspended access waveguides that are terminated by inverted tapers.[16] Figure 4 shows the transmission spectra of the W0.66 waveguide measured with a broad spontaneous emission source and with an optical spectrum analyzer (OSA) near the high- (left) and low- (right) frequency cutoff of the waveguide. Because of the mode mismatch between the W0.66 and the access waveguide at the low-frequency cutoff, the W0.66 waveguide behaves like a Fabry-Perot cavity whose resonant modes are clearly seen. The resonance at 1692.5 nm is used for the Stokes mode and its Q factor is $Q_s=1.8\times10^4$. The group velocity at the pump wavelength (i.e., at 1555.5 nm) is equal to 12 and the Q factor of the pump mode is equal to $Q_p=2400$. The inset of Fig. 4 shows an enlarged view of the transmission spectrum.

To observe the Raman scattering, a tunable laser source and an erbium-doped fiber amplifier are used. Band-pass filters allow to remove the spontaneous emission from the input pump signal as well as to remove the pump wavelength

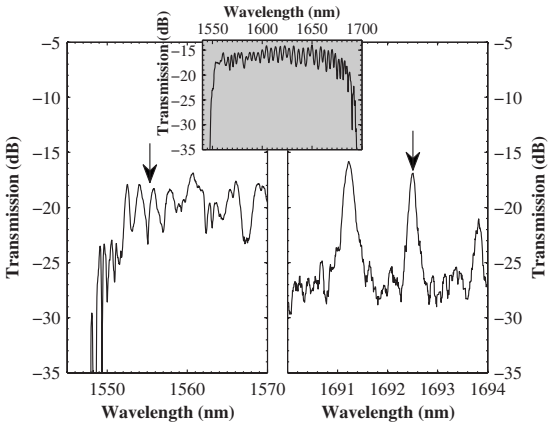

FIG. 4. Transmission spectrum of the W0.66 waveguide with its access waveguides near the high- (left) and low- (right) frequency cutoff (OSA resolution 0.1 nm). The pump (left) and Stokes (right) wavelengths are indicated by an arrow. Inset: whole transmission spectrum (OSA resolution 2 nm).

from the output signal. As expected and contrary to our previous measurements on ridge waveguides oriented along the [110] crystallographic directions of silicon,[4,10] we do not observe any Raman scattering in the access waveguides for input pump power up to 25 mW. A strong Raman scattering was measured in the W0.66 waveguide for a pump wavelength of 1555.5 nm. Figure 5 (left) shows the dependence of the Raman power generated inside the W0.66 waveguide as a function of the pump power at the cavity exit. The collected power is measured in a 1 nm bandwidth and is corrected by taking into account the propagation losses and the coupling losses at the inverted taper tip measured to be equal to 7 dB per side for both the pump and the Stokes wavelengths. The measurement of the pump power is made at the exit of the waveguide because this power is proportional to the pump power circulating inside the cavity and because the Stokes and the pump wavelength have the same coupling losses at the output. The Stokes power linearly depends on the pump power at low excitation as indicated by the dashed line that is

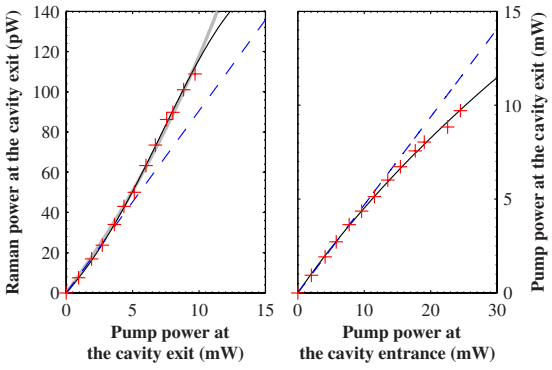

FIG. 5. (Color online) left: measured Stokes power as a function of pump power at the exit of the cavity. Right: pump power at the exit of the cavity as a function of pump power at the entrance of the cavity. The crosses are the measurements while the dashed lines are a linear fit on the five first measurement points at low power. The continuous black curves are nonlinear fits. The gray thick curve is a nonlinear fit that does not take into account the FCA effects.

a linear fit to the five first measurement points. At higher power, the dependence is clearly superlinear indicating that stimulated Raman scattering occurs. At the same time, two photon absorption and photogenerated free-carrier absorption (FCA) start to appear as seen in Fig. 5 (right), that shows a sublinear dependence of the output pump power with the input power.

We now compare these results with calculated Raman gain accounting for FCA. To do so, we introduce the mean number of Stokes photon N_s generated in a cavity by the Raman scattering of N_p pump photons. The number of Stokes photons is related to the collected Stokes power P_s^{out} by $P_s^{\text{out}}=\kappa_s N_s=1/2\sqrt{T_s}N_s\hbar\omega_{s(p)}/\tau_s$, where T_s is the transmission at low power of the cavity at the Stokes wavelength λ_s, $\omega_s=c/\lambda_s$ is the pulsation and $\tau_s=Q_s/\omega_s$ is the Stokes photon lifetime in the resonator. Similar definitions hold for the pump mode. The pump and Stokes photon numbers are related by the following equation:[9,10,17]

$$\frac{dN_s}{dt}=-\frac{N_s}{\tau_s}-\gamma_s^{\text{FCA}}N_p^2N_s+GN_p(N_s+1), \tag{1}$$

where $G=\hbar\omega_p g_R^B c^2/(n_p n_s V_R)$ is the stimulated Raman-scattering gain with $g_R^B=57$ cm GW^{-1} the bulk gain coefficient.[10,12] $\gamma_s^{\text{FCA}}=[\tau^{\text{FC}}c^3\sigma\beta(\hbar\omega_p)^2]/[2n^3\hbar\omega_p(V_s^{\text{FCA}})^2]$ is the absorption rate of the Stokes mode due to pump-generated free-carrier absorption with $\tau^{\text{FC}}=1$ ns the free-carrier lifetime, $\sigma=1.45\times10^{-21}$ m^2 the material-dependent free-carrier absorption cross-section and $\beta=0.84$ cm GW^{-1} the two photon absorption coefficient in silicon.[17] The free-carrier absorption volume of the Stokes mode is given by[9]

$$(V_s^{\text{FCA}})^2=\frac{\left[\int\varepsilon_s(\mathbf{r})|\mathbf{E}_s(\mathbf{r})|^2d^3r\right]\left[\int\varepsilon_p(\mathbf{r})|\mathbf{E}_p(\mathbf{r})|^2d^3r\right]^2}{n_p^4n_s^2\int_{\text{Si}}|\mathbf{E}_s(\mathbf{r})|^2|\mathbf{E}_p(\mathbf{r})|^4d^3r}.$$

Since we are below laser threshold (i.e., $N_s<1$), we have neglected the two photon absorption involving Stokes photons in Eq. (1). In steady state, we have $N_s=G\tau_sN_p/(1-G\tau_sN_p+\gamma_s^{\text{FCA}}\tau_sN_p^2)$ or equivalently

$$P_s^{\text{out}}=\frac{\kappa_sG\tau_s\kappa_p^{-1}P_p^{\text{out}}}{(1-G\tau_s\kappa_p^{-1}P_p^{\text{out}}+\gamma_s^{\text{FCA}}\tau_s\kappa_p^{-2}P_p^{\text{out2}})}.$$

From a nonlinear fit (Fig. 5, left), we get $G\tau_s\kappa_p^{-1}=71$ W^{-1} and, from the measured values, $Q_s=18000$, $Q_p=2400$, and $T_p=0.46$, we get $G=9.5\times10^4$ s^{-1} and $\gamma_s^{\text{FCA}}=0.1$ s^{-1}. This gain corresponds to a Purcell factor $F=G\tau_R$ equal to 1.3, a value higher than the one we have obtained in 25-μm-long W1 waveguides where τ_R^{-1} is the Raman-scattering rate in bulk silicon.[10]

The values of the Raman and FCA volumes have been estimated to be $V_r=1.3\times10^{-17}$ m^3 and $V_s^{\text{FCA}}=5\times10^{-18}$ m^3 with 2D and 3D finite difference in time domain simulations using an homemade code.[18] The calculated Raman gain G and FCA rate γ_s^{FCA} are equal to 4.5×10^4 s^{-1} and 0.015 s^{-1}, respectively. These values are in good agreement with the ones extracted from the fit although they are smaller than the experimental one. These differences can be explained by the

fact that, at low group velocity, localization effects may appear due to disorder in the fabricated structure.[19] This phenomenon can affect both the slow group-velocity pump and Stokes modes and results in effective Raman and FCA volumes smaller than the simulated one. Moreover, we did not try to adjust the value of the free-carrier lifetime τ^{FC}. An other explanation is that for the power range corresponding to the measurements, the free-carrier effect remains relatively low and the fit is not extremely accurate. If the nonlinear fit is done without taking into account the FCA (Fig. 5, left thick gray line), i.e., assuming the following dependence of the Stokes and pump photon numbers, $N_s = G\tau_s N_p/(1 - G\tau_s N_p)$, the measured Raman gain is lower and equal to $G = 3.5 \times 10^4$, which represents a lower limit. Moreover, if the FCA would remain negligible, we can predict a moderate laser threshold equal to $P_p^{\text{out,thres}} = \kappa_p G^{-1} \tau_s^{-1} = 31$ mW. This shows that a silicon PhC Raman laser can be achieved in the same way as PhC waveguides lasers have already been achieved in III-V materials.[20,21] One way to reach the laser threshold in presence of FCA will consist in increasing the currently relatively modest quality factor of the Stokes mode from 1.8×10^4 to 2×10^5 to get a threshold around 3 mW. This can be achieved by fabricating an heterostructure cavity based on such a narrow waveguide.

In conclusion, we have shown that stimulated Raman scattering occurs in narrow silicon photonic crystal waveguides. These waveguides are oriented along the [100] crystallographic direction of silicon and lead to a 60% decrease in the Raman volume as compared to W1 waveguides oriented along the [110] direction. These waveguides also allow a decrease in both the pump and Stokes modes group velocities. For such a structure, stimulated Raman scattering has been observed at room temperature for a continuous incident power as low as 20 mW. This result, in good agreement with the simulations, allows us to predict a laser threshold below 100 mW if the free-carrier absorption could be made negligible.

We thank the Région and C'nano Ile de France for financial support of Zheng Han. We thank M. El Kurdi for fruitful discussions on the fabrication processes.

*xavier.checoury@ief.u-psud.fr

[1] K. Inoue, H. Oda, A. Yamanaka, N. Ikeda, H. Kawashima, Y. Sugimoto, and K. Asakawa, Phys. Rev. A **78**, 011805(R) (2008).

[2] H. Oda, K. Inoue, A. Yamanaka, N. Ikeda, Y. Sugimoto, and K. Asakawa, Appl. Phys. Lett. **93**, 051114 (2008).

[3] J. F. McMillan, M. B. Yu, D. L. Kwong, and C. W. Wong, Appl. Phys. Lett. **93**, 251105 (2008).

[4] X. Checoury, M. El Kurdi, Z. Han, and P. Boucaud, Opt. Express **17**, 3500 (2009).

[5] O. Boyraz and B. Jalali, Opt. Express **12**, 5269 (2004).

[6] H. S. Rong, R. Jones, A. S. Liu, O. Cohen, D. Hak, A. Fang, and M. Paniccia, Nature (London) **433**, 725 (2005).

[7] X. G. Chen, N. C. Panoiu, and R. M. Osgood, IEEE J. Sel. Top. Quantum Electron. **42**, 160 (2006).

[8] T. J. Kippenberg, S. A. Spillane, B. Min, and K. J. Vahala, IEEE J. Sel. Top. Quantum Electron. **10**, 1219 (2004).

[9] X. D. Yang and C. W. Wong, Opt. Express **15**, 4763 (2007).

[10] X. Checoury, Z. Han, M. El Kurdi, and P. Boucaud, Phys. Rev. A **81**, 033832 (2010).

[11] B. Jalali, V. Raghunathan, D. Dimitropoulos, and O. Boyraz, IEEE J. Sel. Top. Quantum Electron. **12**, 412 (2006).

[12] J. I. Dadap, R. L. Espinola, R. M. Osgood, S. J. McNab, and Y. A. Vlasov, Opt. Lett. **29**, 2755 (2004).

[13] R. L. Espinola, J. I. Dadap, R. M. Osgood, S. J. McNab, and Y. A. Vlasov, Opt. Express **12**, 3713 (2004).

[14] J. E. McMillan, X. D. Yang, N. C. Panoiu, R. M. Osgood, and C. W. Wong, Opt. Lett. **31**, 1235 (2006).

[15] J. B. Driscoll, X. P. Liu, S. Yasseri, I. Hsieh, J. I. Dadap, and R. M. Osgood, Opt. Express **17**, 2797 (2009).

[16] Z. Han, X. Checoury, D. Néel, S. David, M. El Kurdi, and P. Boucaud, Opt. Commun. (to be published).

[17] P. Barclay, K. Srinivasan, and O. Painter, Opt. Express **13**, 801 (2005).

[18] X. Checoury, S. Enoch, C. Lopez, and A. Blanco, Appl. Phys. Lett. **90**, 161131 (2007).

[19] J. Topolancik, B. Ilic, and F. Vollmer, Phys. Rev. Lett. **99**, 253901 (2007).

[20] X. Checoury, P. Boucaud, J. M. Lourtioz, F. Pommereau, C. Cuisin, E. Derouin, O. Drisse, L. Legouezigou, F. Lelarge, F. Poingt, G. H. Duan, D. Mulin, S. Bonnefont, O. Gauthier-Lafaye, J. Valentin, F. Lozes, and A. Talneau, Appl. Phys. Lett. **85**, 5502 (2004).

[21] X. Checoury, P. Boucaud, J. M. Lourtioz, O. Gauthier-Lafaye, S. Bonnefont, D. Mulin, J. Valentin, F. Lozes-Dupuy, F. Pommereau, C. Cuisin, E. Derouin, O. Drisse, L. Legouezigou, F. Lelarge, F. Poingt, G. H. Duan, and A. Talneau, Appl. Phys. Lett. **86**, 151111 (2005).